Linear and nonlinear response of a rotating tokamak plasma to a resonant error-field

Richard Fitzpatrick

Citation: Physics of Plasmas (1994-present) **21**, 092513 (2014); doi: 10.1063/1.4896244
View online: http://dx.doi.org/10.1063/1.4896244
View Table of Contents: http://scitation.aip.org/content/aip/journal/pop/21/9?ver=pdfcov
Published by the AIP Publishing

Linear and nonlinear response of a rotating tokamak plasma to a resonant error-field

Richard Fitzpatrick
Department of Physics, Institute for Fusion Studies, University of Texas at Austin, Austin, Texas 78712, USA

(Received 30 May 2014; accepted 8 September 2014; published online 23 September 2014)

An in-depth investigation of the effect of a resonant error-field on a rotating, quasi-cylindrical, tokamak plasma is preformed within the context of constant-ψ, resistive-magnetohydrodynamical theory. General expressions for the response of the plasma at the rational surface to the error-field are derived in both the linear and nonlinear regimes, and the extents of these regimes mapped out in parameter space. Torque-balance equations are also obtained in both regimes. These equations are used to determine the steady-state plasma rotation at the rational surface in the presence of the error-field. It is found that, provided the intrinsic plasma rotation is sufficiently large, the torque-balance equations possess dynamically stable low-rotation and high-rotation solution branches, separated by a forbidden band of dynamically unstable solutions. Moreover, bifurcations between the two stable solution branches are triggered as the amplitude of the error-field is varied. A low- to high-rotation bifurcation is invariably associated with a significant reduction in the width of the magnetic island chain driven at the rational surface, and vice versa. General expressions for the bifurcation thresholds are derived and their domains of validity mapped out in parameter space. [http://dx.doi.org/10.1063/1.4896244]

I. INTRODUCTION

A tokamak is a device whose purpose is to confine a high-temperature plasma on a set of nested toroidal magnetic flux-surfaces. Charged particles are free to circulate rapidly around the flux-surfaces, but can only diffuse slowly across them, as a consequence of their relatively small gyroradii.

The equilibrium magnetic field of a tokamak is supposed to be toroidally symmetric. In reality, there is always a slight deviation from pure toroidal symmetry because of the misalignment of magnetic field coils, the presence of non-axisymmetric current feeds, and so on. It is convenient to describe the field as a superposition of the desired axisymmetric field, $\mathbf{B}$, and an accidentally produced non-axisymmetric "error-field," $\delta\mathbf{B}$.

As a first approximation, a large aspect-ratio, low-β tokamak plasma can be treated as a periodic cylinder of circular cross-section. In such a plasma, the error-field can be decomposed into Fourier harmonics expressed in terms of a (simulated) toroidal angle and a poloidal angle. The typical magnitude of the low mode-number harmonics encountered in present-day tokamaks is about 10^{-4} of the equilibrium toroidal field-strength.

The Fourier harmonics of the error-field fall into two classes, i.e., *resonant* and *non-resonant* harmonics. For a resonant harmonic, there exists at least one so-called *rational* magnetic flux-surface, lying within the plasma, on which $\mathbf{k}\cdot\mathbf{B} = 0$, where $\mathbf{k}$ is a helical wavevector. Conversely, for a non-resonant harmonic, there exists no flux-surface, lying within the plasma, on which $\mathbf{k}\cdot\mathbf{B} = 0$.

The non-resonant harmonics of the error-field give rise to a non-axisymmetric displacement of a tokamak's nested toroidal magnetic flux-surfaces, but do not modify the topology of these surfaces. On the other hand, a resonant harmonic is capable of changing the topology of the flux-surfaces in the immediate vicinity of its associated rational surface, to produce a *helical magnetic island chain*. This process involves *magnetic reconnection* (i.e., the breaking and reforming of magnetic field-lines) at the rational surface. The radial width of the island chain, expressed as a fraction of the plasma minor radius, is of order the square-root of the ratio of the local strength of the resonant harmonic to that of the equilibrium toroidal magnetic field.[1] It follows that relatively small-amplitude resonant harmonics are capable of driving relatively wide island chains. This is problematic, because a helical magnetic island chain degrades the confinement properties of the plasma equilibrium by allowing heat and particles to flow rapidly, rather than diffuse slowly, from the inner to the outer (radial) sides of its associated magnetic separatrix.[2]

One would naively expect a tokamak plasma subject to an error-field to be filled with magnetic island chains induced by the various resonant harmonics of the field. Fortunately, this is not necessarily the case. Tokamak plasmas generally rotate, due to the presence of an equilibrium radial electric field (as well as diamagnetic effects), at a rate that is far larger than that at which magnetic reconnection typically proceeds. Under these circumstances, driven magnetic reconnection at the various rational surfaces within the plasma is largely suppressed, and the confinement properties of the plasma remain unimpaired.[3,4] Unfortunately, even in the presence of substantial plasma rotation, a residual amount of magnetic reconnection is driven at each rational surface within the plasma. Moreover, this residual reconnection gives rise to localized electromagnetic torques that acts to decelerate the rotation.[3,4] Under these circumstances, it is not at all obvious that a

tokamak plasma, subject to a given error-field, can maintain sufficient rotation to suppress driven magnetic reconnection, and thereby prevent any error-field-induced degradation of its confinement properties.

A resistive-MHD (magnetohydrodynamical) theory of the response of a rotating, quasi-cylindrical, tokamak plasma to a resonant error-field was developed previously in Refs. 3 and 4. Reference 3 makes use of linear layer theory to characterize the response of the plasma in the immediate vicinity of a given rational surface to the associated resonant harmonic of the error-field, and, hence, to determine the deceleration torque acting in the vicinity of the surface. This approach is limited to situations in which the width of the island chain induced at the rational surface is much less than the linear layer width. In Ref. 4, the analysis of Ref. 3 is extended to permit situations in which the width of the driven island chain greatly exceeds the linear layer width. In this case, the response of the plasma in the immediate vicinity of the rational surface, as well as the decoration torque, is determined by nonlinear island theory.[1] The analysis of Refs. 3 and 4 predicts that if the intrinsic (i.e., in the absence of the error-field) plasma rotation is sufficiently rapid then, in the presence of a resonant error-field, there is a forbidden band of plasma rotation frequencies which separates relatively high-rotation from relatively low-rotation states. Moreover, bifurcations between high- and low-rotation states are triggered as the amplitude of the resonant harmonic of the error-field is varied. A high- to low-rotation bifurcation is invariably associated with a significant increase in the driven island width, and vice versa.

The aim of this paper is to perform an in-depth investigation of the bifurcated states of a rotating, quasi-cylindrical, tokamak plasma in the presence of a resonant error-field, within the context of constant-ψ,[5] resistive-MHD theory. Incidentally, we are restricting our investigation to constant-ψ response regimes because it was demonstrated in Ref. 4 that these are the most appropriate regimes in ohmically heated tokamak plasmas. The analysis presented here is much more general than that given in Refs. 3 and 4 (other than the restriction to constant-ψ response regimes) because we do not necessarily assume that the plasma is rapidly rotating, and also do not concentrate exclusively on high- to low-rotation bifurcations.

II. PRELIMINARY ANALYSIS

A. Plasma equilibrium

Consider a large aspect-ratio, low-β, tokamak plasma whose magnetic flux surfaces map out (almost) concentric circles in the poloidal plane. Such a plasma is well approximated as a periodic cylinder. Suppose that the minor radius of the plasma is a. Standard cylindrical coordinates (r, θ, z) are adopted. The system is assumed to be periodic in the z-direction, with periodicity length $2\pi R_0$, where $R_0 \gg a$ is the simulated plasma major radius. It is convenient to define the simulated toroidal angle $\phi = z/R_0$.

The equilibrium magnetic field is written $\mathbf{B} = [0, B_\theta(r), B_\phi]$. The associated equilibrium plasma current density takes the form $\mathbf{j} = [0, 0, j_\phi(r)]$, where

$$\mu_0 j_\phi(r) = \frac{1}{r}\frac{d(r B_\theta)}{dr}. \tag{1}$$

The safety factor,

$$q(r) = \frac{r B_\theta}{R_0 B_\phi}, \tag{2}$$

parameterizes the helical pitch of equilibrium magnetic field-lines. In a conventional tokamak plasma, $q(r)$ is of order unity, and is a monotonically increasing function of r.

B. Plasma response

Consider the response of the plasma to a static, helical, magnetic perturbation, which is, henceforth, referred to as an error-field (although it actually only represents one particular resonant harmonic of the total error-field). Suppose that the error-field has m periods in the poloidal direction, and n periods in the toroidal direction. It is convenient to express the perturbed magnetic field and the perturbed plasma current density in terms of a magnetic flux-function, $\psi(r, \theta, \phi, t)$. Thus,

$$\delta\mathbf{B} = \nabla\psi \times \mathbf{e}_z, \tag{3}$$

$$\mu_0\, \delta\mathbf{j} = -\nabla^2\psi\, \mathbf{e}_z, \tag{4}$$

where

$$\psi(r, \theta, \phi, t) = \hat{\psi}(r, t)\, \exp[\mathrm{i}\,(m\,\theta - n\,\phi)]. \tag{5}$$

This representation is valid provided that[3]

$$\frac{m}{n} \gg \frac{a}{R_0}. \tag{6}$$

As is well known, the response of the plasma to the applied error-field is governed by the equations of perturbed, marginally stable (i.e., $\partial/\partial t \equiv 0$), ideal MHD everywhere in the plasma, apart from a relatively narrow (in r) region in the vicinity of the rational surface, minor radius r_s, where $q(r_s) = m/n$.[3]

It is convenient to parameterize the error-field in terms of the so-called *vacuum flux*, $\Psi_v(t) = |\Psi_v|\, \mathrm{e}^{-\mathrm{i}\,\varphi_v}$, which is defined to be the value of $\hat{\psi}(r, t)$ at radius r_s in the presence of the error-field, but in the absence of the plasma. Here, φ_v is the helical phase of the error-field. Likewise, the response of the plasma in the vicinity of the rational surface to the error-field is parameterized in terms of the so-called *reconnected flux*, $\Psi_s(t) = |\Psi_s|\, \mathrm{e}^{-\mathrm{i}\,\varphi_s}$, which is the actual value of $\hat{\psi}(r, t)$ at radius r_s. Here, φ_s is the helical phase of the reconnected flux.

The intrinsic stability of the m, n tearing mode is governed by the *tearing stability index*,

$$\Delta' = \left[\frac{d\ln\hat{\psi}}{d\ln r}\right]_{r_s-}^{r_s+}, \tag{7}$$

where $\hat{\psi}(r)$ is a solution of the marginally stable, ideal-MHD equations, for the case of an m, n helical perturbation, that

satisfies physical boundary conditions at $r=0$ and $r=a$ (in the absence of the error-field). According to resistive-MHD theory,[1,5] if $\Delta' > 0$ then the m, n tearing mode spontaneously reconnects magnetic flux at the rational surface to form a helical magnetic island chain. In the following, it is assumed that $\Delta' < 0$, so that the m, n tearing mode is intrinsically stable. In this situation, any magnetic reconnection that takes place at the rational surface is due solely to the error-field.

C. Linear regime

In this paper, we shall examine two different constant-ψ, resistive-MHD response regimes at the rational surface. The first of these is the so-called visco-resistive regime.[3,4] This is a *linear* regime in which the reconnected magnetic flux induced by the error-field is governed by (see Appendix A)

$$\frac{\delta_{\rm VR}}{r_s}\,\tau_R\left(\frac{d}{dt}+{\rm i}\,\omega\right)\Psi_s=\Delta'\,\Psi_s+2\,m\,\Psi_v. \tag{8}$$

Here,

$$\delta_{\rm VR}=2.104\left(\frac{\tau_H^{\,1/3}}{\tau_R^{\,1/6}\,\tau_V^{\,1/6}}\right)r_s, \tag{9}$$

is the linear layer width, whereas

$$\tau_H=\frac{R_0}{B_\phi}\,\frac{\sqrt{\mu_0\,\rho(r_s)}}{n\,s}, \tag{10}$$

$$\tau_R=\mu_0\,r_s^2\,\sigma(r_s), \tag{11}$$

$$\tau_V=\frac{r_s^2\,\rho(r_s)}{\mu(r_s)}, \tag{12}$$

are the hydromagnetic, resistive diffusion, and viscous diffusion timescales, respectively, at the rational surface. Moreover, $s=(d\ln q/d\ln r)_{r_s}$ is the local magnetic shear, and $\rho(r)$, $\sigma(r)$, $\mu(r)$ are the equilibrium plasma mass density, electrical conductivity, and (perpendicular) viscosity profiles, respectively. Finally,

$$\omega=m\,\Omega_\theta(r_s)-n\,\Omega_\phi(r_s), \tag{13}$$

where $\Omega_\theta(r)$ and $\Omega_\phi(r)$ are the equilibrium plasma poloidal and toroidal angular velocity profiles, respectively.

It is easily demonstrated that zero net electromagnetic torque can be exerted on magnetic flux surfaces located in a region of the plasma that is governed by the equations of marginally stable, ideal MHD.[3] Thus, any electromagnetic torque exerted on the plasma by the error-field develops in the immediate vicinity of the rational surface, where ideal MHD breaks down. In the linear regime, the net toroidal electromagnetic torque exerted in the vicinity of the rational surface by the error-field takes the form[3,4]

$$T_{\phi\,\rm EM}=\frac{4\pi^2\,n\,m\,R_0}{\mu_0}\left(\frac{2\,m}{-\Delta'}\right)|\Psi_v|^2\,T, \tag{14}$$

where

$$T=\left(\frac{-\Delta'}{2\,m}\right)\frac{|\Psi_s|}{|\Psi_v|}\,\sin(\varphi_s-\varphi_v). \tag{15}$$

D. Nonlinear regime

The second response regime investigated in this paper is the so-called Rutherford regime.[4] This is a *nonlinear* regime in which the reconnected magnetic flux induced by the error-field is governed by two equations. The first of these is the *Rutherford island width evolution equation*,[1]

$$0.8227\,\tau_R\,\frac{d}{dt}\left(\frac{W}{r_s}\right)=\Delta'+2\,m\left(\frac{W_v}{W}\right)^2\cos(\varphi_s-\varphi_v). \tag{16}$$

Here,

$$W=4\left(\frac{|\Psi_s|}{s\,r_s\,B_\theta(r_s)}\right)^{1/2}r_s, \tag{17}$$

is the full (radial) width of the magnetic island chain that forms at the rational surface, and $B_\theta(r_s)=r_s\,B_\phi/R_0\,q(r_s)$ is the local equilibrium poloidal magnetic field. Finally,

$$W_v=4\left(\frac{|\Psi_v|}{s\,r_s\,B_\theta(r_s)}\right)^{1/2}r_s, \tag{18}$$

is termed the vacuum island width. The second governing equation is the so-called *no-slip constraint*,[3]

$$\frac{d\varphi_s}{dt}-\omega=0, \tag{19}$$

according to which the island chain is forced to co-rotate with the plasma at the rational surface. The net toroidal electromagnetic torque exerted by the error-field in the vicinity of the rational surface is again given by Eqs. (14) and (15).

The nonlinear regime holds when

$$W\gg\delta_{\rm VR}, \tag{20}$$

i.e., when the magnetic island width greatly exceeds the linear layer width. The linear regime holds in the opposite case in which the island width falls well below the linear layer width. In addition, the particular linear regime employed in this paper (i.e., the visco-resistive regime) is only valid when $\omega\ll(\tau_R/\tau_V^2\,\tau_H^2)^{1/3}$, $(\tau_V/\tau_R^2\,\tau_H^2)^{1/3}$ (i.e., when the constant-ψ approximation holds).[4] Likewise, the particular nonlinear regime employed in this paper (i.e., the Rutherford regime) is only valid when $2m\,(W/r_s)\,(W_v/W)^2\ll 1$ (i.e., when the constant-ψ approximation holds).[4]

E. Normalization scheme

Without loss of generality, we can set $\varphi_v=0$. Let

$$\hat{W}=\frac{0.8227}{2}\,\frac{W}{\delta_{\rm VR}}, \tag{21}$$

$$\hat{W}_v = \frac{0.8227}{2}\,\frac{W_v}{\delta_{\rm VR}}\left(\frac{2\,m}{-\Delta'}\right)^{1/2}, \tag{22}$$

$$\hat{t} = \left(\frac{r_s}{\delta_{\rm VR}}\,\frac{-\Delta'}{\tau_R}\right) t, \tag{23}$$

$$\hat{\omega} = \left(\frac{\delta_{\rm VR}}{r_s}\,\frac{\tau_R}{-\Delta'}\right)\omega. \tag{24}$$

Equation (8), which governs the response of the plasma to the error-field in the linear regime, yields (see Appendix A)

$$\frac{d\hat{W}}{d\hat{t}} = \frac{\hat{W}}{2}\left(-1 + \frac{\hat{W}_v^2}{\hat{W}^2}\,\cos\varphi\right), \tag{25}$$

$$\frac{d\varphi}{d\hat{t}} - \hat{\omega} = -\frac{\hat{W}_v^2}{\hat{W}^2}\,\sin\varphi, \tag{26}$$

where $\varphi = \varphi_s - \varphi_v$ is the helical phase of the island chain relative to the error-field. On the other hand, Eqs. (16) and (19), which govern the plasma response in the nonlinear regime, give

$$\frac{d\hat{W}}{d\hat{t}} = \frac{1}{2}\left(-1 + \frac{\hat{W}_v^2}{\hat{W}^2}\,\cos\varphi\right), \tag{27}$$

$$\frac{d\varphi}{d\hat{t}} - \hat{\omega} = 0. \tag{28}$$

Equations (25) and (26) hold when

$$\hat{W} \ll 1, \tag{29}$$

whereas Eqs. (27) and (28) hold when

$$\hat{W} \gg 1. \tag{30}$$

In both cases, the normalized toroidal electromagnetic torque exerted in the vicinity of the rational surface takes the form

$$T = \left(\frac{\hat{W}}{\hat{W}_v}\right)^2 \sin\varphi. \tag{31}$$

It is interesting to note that Eq. (25), which governs the island width evolution in the linear regime, is fairly similar in form to Eq. (27), which governs the island width evolution in the nonlinear regime. On the other hand, Eq. (26), which governs the evolution of the island phase in the linear regime, is substantially different to Eq. (28), which governs the evolution of the island phase in the nonlinear regime. According to Eq. (28), a nonlinear magnetic island chain (i.e., a chain whose width greatly exceeds the linear layer width) is forced to co-rotate with the plasma at the rational surface. (Essentially, this is because the island chain is too wide for plasma to easily diffuse across, leading to the trapping of plasma within the chain's magnetic separatrix.) On the other hand, according to Eq. (26), a linear island chain (i.e., a chain whose width is much less than the linear layer width) can slip through the plasma at the rational surface. In fact, the right-hand side of Eq. (26) represents the normalized *slip frequency* (i.e., the difference between the chain's angular rotation frequency and that of the plasma at the rational surface).

According to Eqs. (25) and (27), the error-field destabilizes the island chain when $\cos\varphi > 0$ (i.e., when $-\pi/2 < \varphi < \pi/2$), and stabilizes the chain otherwise. Moreover, according to Eq. (31), the toroidal electromagnetic torque exerted by the error-field acts to decelerate the plasma rotation at the rational surface (i.e., $T > 0$) when $\sin\varphi > 0$ (i.e., when $0 < \varphi < \pi$), and acts to accelerate the rotation otherwise.

III. LINEAR RESPONSE THEORY

A. Introduction

This section investigates the linear response of a rotating plasma to an error-field.

B. Phase-space evolution

It is helpful to define

$$X = \hat{W}^2\,\cos\varphi, \tag{32}$$

$$Y = \hat{W}^2\,\sin\varphi. \tag{33}$$

Here, X is the component of the normalized, error-field-driven, reconnected magnetic flux that is in-phase with the error-field, whereas Y is the corresponding component that is in phase-quadrature. The linear response equations, (25) and (26), can be rewritten in the form

$$\frac{dX}{d\hat{t}} = -X - \hat{\omega}\,Y + \hat{W}_v^2, \tag{34}$$

$$\frac{dY}{d\hat{t}} = -Y + \hat{\omega}\,X. \tag{35}$$

It follows that the response of the plasma to the error-field can be visualized as a trajectory in X-Y space. Henceforth, X-Y space is termed *phase-space*. In fact, Eqs. (34) and (35) can be solved to give

$$X(t) = \left(\frac{1}{1+\hat{\omega}^2}\right)\hat{W}_v^2\left(1 - [\cos(\hat{\omega}\,\hat{t}) - \hat{\omega}\,\sin(\hat{\omega}\,\hat{t})]\,{\rm e}^{-\hat{t}}\right) + \left[X(0)\cos(\hat{\omega}\,\hat{t}) - Y(0)\sin(\hat{\omega}\,\hat{t})\right]{\rm e}^{-\hat{t}}, \tag{36}$$

$$Y(t) = \left(\frac{1}{1+\hat{\omega}^2}\right)\hat{W}_v^2\left(\hat{\omega} - [\hat{\omega}\,\cos(\hat{\omega}\,\hat{t}) + \sin(\hat{\omega}\,\hat{t})]\,{\rm e}^{-\hat{t}}\right) + \left[Y(0)\cos(\hat{\omega}\,\hat{t}) + X(0)\sin(\hat{\omega}\,\hat{t})\right]{\rm e}^{-\hat{t}}. \tag{37}$$

It is, thus, clear that the phase-space trajectory takes the form of an exponential decay to the *fixed point*

$$X(\infty) = \left(\frac{1}{1+\hat{\omega}^2}\right)\hat{W}_v^2, \tag{38}$$

$$Y(\infty) = \left(\frac{\hat{\omega}}{1+\hat{\omega}^2}\right)\hat{W}_v^2. \tag{39}$$

A typical phase-space trajectory in the linear regime is shown in Fig. 1.

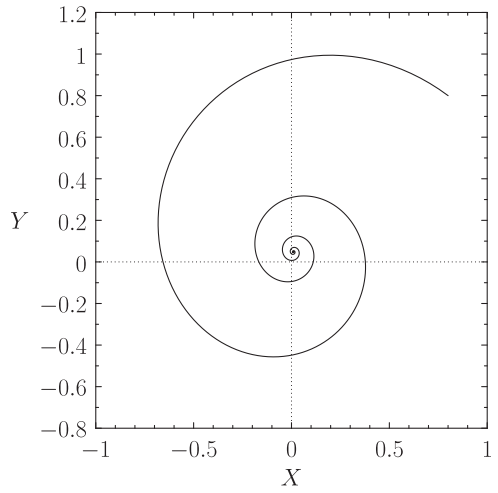

FIG. 1. Phase-space evolution of the reconnected flux induced in a rotating tokamak plasma by a resonant error-field in the linear response regime. The parameters for this plot are $\hat{\omega} = 5$, $\hat{W}_v = 0.5$, $X(0) = 0.8$, and $Y(0) = 0.8$.

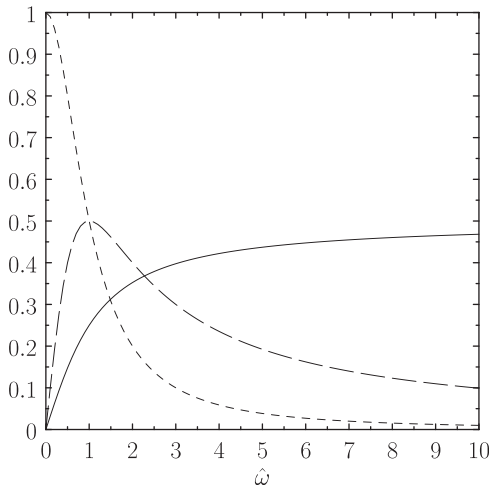

FIG. 2. Time-asymptotic linear response of a rotating tokamak plasma to a resonant error-field plotted as a function of the normalized rotation frequency at the rational surface, $\hat{\omega}$. The solid, short-dashed, and long-dashed curves show φ/π, $(\hat{W}/\hat{W}_v)^4$, and T, respectively.

C. Time-asymptotic response

At the fixed point, which clearly corresponds to the time-asymptotic linear response of the plasma to the error-field,

$$\varphi = \tan^{-1}(\hat{\omega}), \tag{40}$$

$$\left(\frac{\hat{W}}{\hat{W}_v}\right)^4 = \frac{1}{1+\hat{\omega}^2}, \tag{41}$$

$$T = \frac{\hat{\omega}}{1+\hat{\omega}^2}. \tag{42}$$

This response is characterized by a non-rotating (i.e., $d\varphi/d\hat{t} = 0$) island chain of fixed width (that is much less than the linear layer width). Moreover, the plasma at the rational surface flows through the island chain, i.e., $d\varphi/d\hat{t} - \hat{\omega} \neq 0$. Finally, this flow gives rise to a fixed helical phase-shift, φ, of the chain with respect to the vacuum island chain (i.e., the island chain obtained by naively superimposing the vacuum error-field perturbation onto the plasma equilibrium).

The time-asymptotic linear response of the plasma to the error-field, which is specified by Eqs. (40)–(42), is further illustrated in Fig. 2. It can be seen that, in the absence of plasma rotation (i.e., $\hat{\omega} = 0$), the island chain is locked in-phase with the error-field (i.e., $\varphi = 0$), and achieves its maximum possible width, $\hat{W} = \hat{W}_v$. In the presence of finite plasma rotation (i.e., $\hat{\omega} > 0$), the island chain is phase-shifted with respect to the error-field (i.e., $\varphi > 0$), and its width is reduced (i.e., $\hat{W} < \hat{W}_v$). In the limit of strong plasma rotation (i.e., $\hat{\omega} \gg 1$), the phase-shift approaches $\pi/2$, and the reduction in the driven island width becomes substantial (i.e., $\hat{W} \ll \hat{W}_v$). It can also be seen that the toroidal electromagnetic torque exerted by the error-field acts to decelerate the plasma rotation at the rational surface (i.e., $T > 0$). Moreover, this torque is a non-monotonic function of the normalized plasma rotation frequency, $\hat{\omega}$, approaching zero in the limits $\hat{\omega} \to 0$ and $\hat{\omega} \to \infty$, and peaking at $\hat{\omega} = 1$.

In the limit of strong plasma rotation, the time-asymptotic linear response just described has many features in common with the *small locked island regime* discussed in Refs. 7–9.

Finally, because the linear regime is only valid when $\hat{W} \ll 1$ (i.e., when the island width falls well below the linear layer width), it follows from Eq. (41) that the time-asymptotic response of the plasma to the error-field only lies in the linear regime when

$$\hat{W}_v \ll (1+\hat{\omega}^2)^{1/4}. \tag{43}$$

IV. NONLINEAR RESPONSE THEORY

A. Introduction

This section investigates the nonlinear response of a rotating plasma to an error-field.

B. Phase-space evolution

Let

$$v = \hat{W}^3. \tag{44}$$

The nonlinear response equations, (27) and (28), can be rewritten in the form

$$\frac{dv}{d\hat{t}} = \frac{3}{2}\left(-v^{2/3} + \hat{W}_v^2 \cos\varphi\right), \tag{45}$$

$$\frac{d\varphi}{d\hat{t}} = \hat{\omega}. \tag{46}$$

As before, the solution of these equations can be visualized as a trajectory in X-Y space, where

$$X = v^{2/3} \cos\varphi, \tag{47}$$

$$Y = v^{2/3} \sin\varphi. \tag{48}$$

In principle, Eq. (45) permits the variable v to pass through zero and become negative, which implies that the normalized island width, $\hat{W}$, also becomes negative. However, a magnetic island chain of negative width is equivalent to a chain of equal and opposite positive width in which the O-points are converted into X-points, and vice versa (such conversion implies a π radian helical phase-shift).[4] In this paper, the island width is defined to be always positive. In order to maintain this definition, when evolving Eqs. (45) and (46), we must make the transformation

$$v \rightarrow -v, \tag{49}$$

$$\varphi \rightarrow \varphi - \pi, \tag{50}$$

each time v passes through zero and becomes negative. This transformation is consistent with the straight-line passage of the corresponding phase-space trajectory through the origin (see Fig. 4).

Figure 3 shows a typical phase-space trajectory in the nonlinear regime. It can be seen that, unlike a typical trajectory in the linear regime, which decays to a fixed point (see Fig. 1), a typical phase-space trajectory in the nonlinear regime asymptotes to a *closed loop* (i.e., a limit cycle) that passes through the origin. (Assuming that $\hat{\omega} > 0$, the time-asymptotic trajectory orbits the loop in a counter-clockwise sense.) The fact that the loop passes through the origin implies that the associated island width, $\hat{W}(\hat{t})$, periodically falls to zero. Each time this occurs, the island phase decreases discontinuously by π radians, in accordance with Eq. (50). Consequently, although the helical phase of the island chain with respect to the error-field, $\varphi(\hat{t})$ is constantly increasing in time at a uniform rate, its value is nevertheless restricted to lie in the limited range

$$\varphi_0 \leq \varphi(\hat{t}) \leq \varphi_0 + \pi, \tag{51}$$

where φ_0 is some constant.

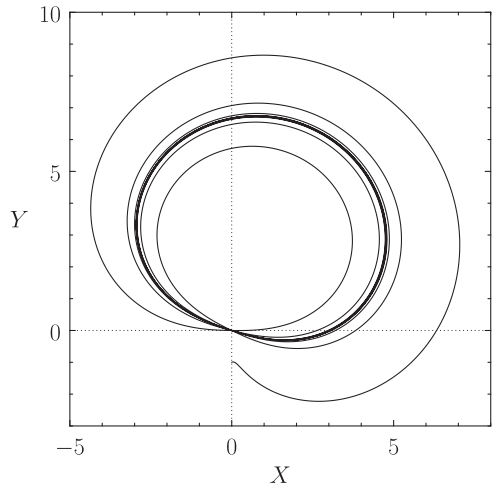

FIG. 3. Phase-space evolution of the reconnected flux induced in a rotating tokamak plasma by a resonant error-field in the nonlinear response regime. The parameters for this plot are $\hat{\omega} = 2$, $\hat{W}_v = 5.0$, $W(0) = 1.0$, and $\varphi(0) = -\pi/2$.

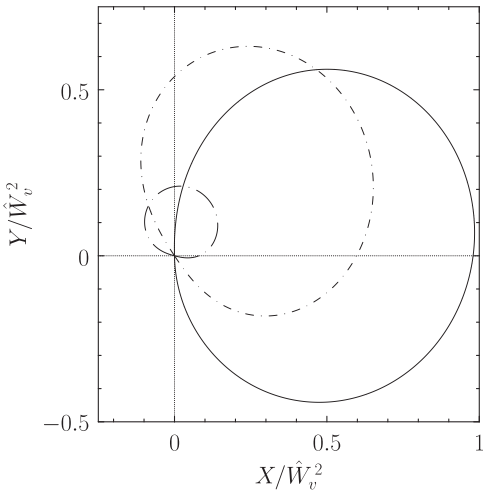

FIG. 4. Time-asymptotic phase-space trajectories in the nonlinear response regime. The solid, short-dashed-dotted, and long-dashed-dotted curves correspond to $\alpha = 0.1$, 1.0, and 10.0, respectively. The corresponding values of φ_0/π are −0.49181, −0.30049, and −0.07617, respectively.

C. Time-asymptotic response

The time-asymptotic solution of the nonlinear equations, (45) and (46), is clearly periodic in $\hat{t}$, with period $\hat{\tau} = \pi/\hat{\omega}$. In other words, $v(\hat{t} + \hat{\tau}) = v(\hat{t})$ and $\varphi(\hat{t} + \hat{\tau}) = \varphi(\hat{t})$ for all $\hat{t}$. Without loss of generality, we can set $\varphi(0) = \varphi_0$. It then follows from Eq. (46) that

$$\varphi(\hat{t}) = \varphi_0 + \hat{\omega}\,\hat{t}, \tag{52}$$

for $0 \leq \hat{t} \leq \hat{\tau}$. Likewise,

$$\hat{t} = \left(\frac{\varphi - \varphi_0}{\pi}\right)\hat{\tau}, \tag{53}$$

for $\varphi_0 \leq \varphi \leq \varphi_0 + \pi$. Clearly, a periodic function of $\hat{t}$, with $\hat{t}$ in the range of $0 \leq \hat{t} \leq \hat{\tau}$, can also be thought of as a function of φ, with φ in the range of $\varphi_0 \leq \varphi \leq \varphi_0 + \pi$. Thus, we can write $v = v(\varphi)$ for $\varphi_0 \leq \varphi \leq \varphi_0 + \pi$. Equations (45) and (46) can then be combined to give

$$\alpha\,\frac{du}{d\varphi} = \cos\varphi - u^{2/3}, \tag{54}$$

where

$$u(\varphi) = \frac{v(\varphi)}{\hat{W}_v^{\,3}}, \tag{55}$$

$$\alpha = \frac{2\,\hat{\omega}\,\hat{W}_v}{3}. \tag{56}$$

Equation (54) must be solved subject to the constraints

$$u(\varphi_0) = 0, \tag{57}$$

$$u(\varphi_0 + \pi) = 0, \tag{58}$$

which ensure that the island chain's width instantaneously passes through zero each time its helical phase decreases

discontinuously from $\varphi_0+\pi$ to φ_0, in accordance with Eqs. (49) and (50). In general, for a given value of α, there is only a single value of the parameter φ_0 that allows the previous two constraints to be simultaneously satisfied. Once φ_0 and $u(\varphi)$ have been determined numerically, we can calculate

$$\left[\frac{\hat{W}(\varphi)}{\hat{W}_v}\right]^4 = u^{4/3}, \tag{59}$$

$$T(\varphi) = u^{2/3}\,\sin\varphi. \tag{60}$$

The solution of Eq. (54), subject to the constraints (57) and (58), is illustrated in Figs. 4–6. The general features of the solution are as follows. In accordance with the no-slip constraint, the helical phase of the island chain, φ, increases linearly in time. The chain's width grows from zero when $\varphi=\varphi_0$, achieves a maximum value when $\varphi\simeq\varphi_0+\pi/2$, and decays to zero again when $\varphi=\varphi_0+\pi$. At this point, the chain's phase decreases abruptly by π radians, and the cycle repeats ad infinitum. Note that the abrupt phase changes correspond to the passage of the associated phase-space trajectory through the origin (see Fig. 4).

The low plasma rotation limit, $\alpha\ll 1$, is characterized by $\varphi_0\simeq-\pi/2$. This implies that, during the island chain's growth/decay cycle, its helical phase always lies in the destabilizing range, $-\pi/2<\varphi<\pi/2$. On the other hand, the phase lies in the accelerating range, $-\pi<\varphi<0$ during half of the cycle, and in the decelerating range, $0<\varphi<\pi$, during the other half. Consequently, in the low plasma rotation limit, the island chain achieves a relatively large peak width, and is subject to alternating accelerating and decelerating electromagnetic torques.

The high plasma rotation limit, $\alpha\gg 1$, is characterized by $\varphi_0\simeq 0$. This implies that the phase of the island chain lies in the destabilizing range, $-\pi/2<\varphi<\pi/2$, during half of its growth/decay cycle, and in the stabilizing range during the other half. On the other hand, the phase always lies in the decelerating range, $0<\varphi<\pi$. Consequently, in the high plasma rotation limit, the island chain only achieves a relatively small peak width, and is subject to a continuously decelerating electromagnetic torque.

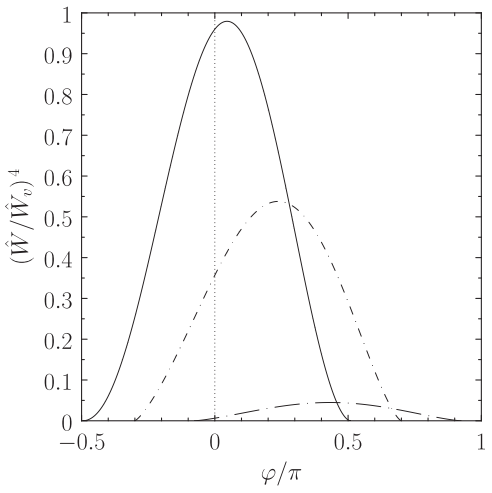

FIG. 5. Time-asymptotic nonlinear response of a rotating tokamak plasma to a resonant error-field. The solid, short-dashed-dotted, and long-dashed-dotted curves show $(\hat{W}/\hat{W}_v)^4$ versus φ/π, calculated for $\alpha=0.1$, $\alpha=1.0$, and $\alpha=10.0$, respectively. The corresponding values of φ_0/π are −0.49181, −0.30049, and −0.07617, respectively.

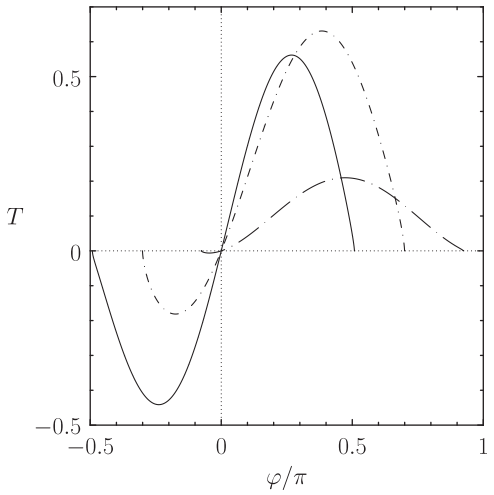

FIG. 6. Time-asymptotic nonlinear response of a rotating tokamak plasma to a resonant error-field. The solid, short-dashed-dotted, and long-dashed-dotted curves show T versus φ/π, calculated for $\alpha=0.1$, $\alpha=1.0$, and $\alpha=10.0$, respectively. The corresponding values of φ_0/π are −0.49181, −0.30049, and −0.07617, respectively.

D. Analytic approximations

It is helpful to define a *cycle average operator*

$$\langle\cdots\rangle\equiv\frac{1}{\pi}\int_{\varphi_0}^{\varphi_0+\pi}(\cdots)\,d\varphi. \tag{61}$$

It immediately follows that

$$\langle\varphi\rangle=\varphi_0+\frac{\pi}{2}. \tag{62}$$

In other words, the mean helical phase of the island chain, during its growth/decay cycle, is $\varphi_0+\pi/2$.

Consider the low plasma rotation limit, $\alpha\ll 1$. Expanding in the small parameter α, the zeroth-order solution to Eq. (54) is

$$u\simeq\cos^{3/2}\varphi. \tag{63}$$

Now, by definition, φ_0 is the negative root of

$$u(\varphi_0)=0. \tag{64}$$

It follows that, to lowest order, $\varphi_0=-\pi/2$. The first-order solution to Eq. (54) is

$$u\simeq\cos^{3/2}\varphi+\frac{9}{4}\,\alpha\,\cos\varphi\,\sin\varphi. \tag{65}$$

Unfortunately, it is not possible to determine the next order correction to φ_0 from Eq. (65), because the expansion upon which this expression is based breaks down close to $\varphi=-\pi/2$. However, an examination of the numerical solution to Eq. (54) reveals that

$$\frac{\varphi_0}{\pi} \simeq -\frac{1}{2} + 0.8235\,\alpha^2, \tag{66}$$

in the limit $\alpha \ll 1$. Hence, making use of Eq. (62),

$$\frac{\langle\varphi\rangle}{\pi} \simeq 0.8235\,\alpha^2. \tag{67}$$

It follows from Eqs. (59), (60), and (65) that, to first order in α,

$$\left(\frac{\hat{W}}{\hat{W}_v}\right)^4 \simeq \cos^2\varphi + 3\,\alpha\,\cos^{3/2}\varphi\,\sin\varphi, \tag{68}$$

$$T \simeq \cos\varphi\,\sin\varphi + \frac{3}{2}\,\alpha\,\cos^{1/2}\varphi\,\sin^2\varphi. \tag{69}$$

Hence, to the same order,

$$\left\langle\left(\frac{\hat{W}}{\hat{W}_v}\right)^4\right\rangle \simeq 0.5, \tag{70}$$

$$\langle T\rangle \simeq \left(\frac{3}{2\,\pi}\int_{-\pi/2}^{\pi/2} \cos^{1/2}\varphi\,\sin^2\varphi\,d\varphi\right)\alpha = 0.4577\,\alpha. \tag{71}$$

Consider the high plasma rotation limit, $\alpha \gg 1$. Expanding in the small parameter α^{-1}, the zeroth-order solution to Eq. (54) is

$$u \simeq \frac{\sin\varphi}{\alpha}. \tag{72}$$

Moreover, the first-order solution is

$$u \simeq \frac{\sin\varphi}{\alpha} + \alpha^{-5/3}\int_{\varphi}^{\pi/2} \sin^{2/3}x\,dx. \tag{73}$$

It follows from Eq. (64) that

$$\frac{\varphi_0}{\pi} \simeq -\left(\frac{1}{\pi}\int_0^{\pi/2} \sin^{2/3}\varphi\,d\varphi\right)\alpha^{-2/3} = -0.3566\,\alpha^{-2/3}. \tag{74}$$

Hence, making use of Eq. (62),

$$\frac{\langle\varphi\rangle}{\pi} \simeq 0.5 - 0.3566\,\alpha^{-2/3}. \tag{75}$$

According to Eqs. (59), (60), and (72), to lowest order in α^{-1},

$$\left(\frac{\hat{W}}{\hat{W}_v}\right)^4 \simeq \frac{\sin^{4/3}\varphi}{\alpha^{4/3}}, \tag{76}$$

$$T \simeq \frac{\sin^{5/3}\varphi}{\alpha^{2/3}}. \tag{77}$$

It follows that, to the same order:

$$\left\langle\left(\frac{\hat{W}}{\hat{W}_v}\right)^4\right\rangle \simeq \left(\frac{1}{\pi}\int_0^{\pi} \sin^{4/3}\varphi\,d\varphi\right)\alpha^{-4/3} = 0.5798\,\alpha^{-4/3}, \tag{78}$$

$$\langle T\rangle \simeq \left(\frac{1}{\pi}\int_0^{\pi} \sin^{5/3}\varphi\,d\varphi\right)\alpha^{-2/3} = 0.5356\,\alpha^{-2/3}. \tag{79}$$

Interpolating between the small-α results (67), (70), and (71), and the large-α results (75), (78), and (79), we obtain the following analytic approximations:

$$\frac{\langle\varphi\rangle}{\pi} \simeq \frac{\alpha^2}{1+2\,\alpha^2} - \frac{0.1756\,\alpha^2}{1+0.4950\,\alpha^{8/3}}, \tag{80}$$

$$\left\langle\left(\frac{\hat{W}}{\hat{W}_v}\right)^4\right\rangle \simeq \frac{0.5}{1+0.8624\,\alpha^{4/3}}, \tag{81}$$

$$\langle T\rangle \simeq \frac{0.4577\,\alpha}{1+0.8546\,\alpha^{5/3}}. \tag{82}$$

In Figs. 7–9, these approximations are compared with to corresponding quantities obtained via the direct numerical solution of Eq. (54). It can be seen that the approximations are fairly accurate. Note, incidentally, that the nonlinear analysis presented in Ref. 4 only considered the high plasma rotation limit, $\alpha \gg 1$. In this paper, we have considerably extended the previous analysis so as to be able to deal with any value of the plasma rotation parameter, α.

Expressions (80)–(82) are the nonlinear equivalents of the linear results (40)–(42). We can see that the plasma response to the error-field in the nonlinear regime is broadly similar in nature to that in the linear regime. To be more precise, in both regimes, as the plasma rotation (parameterized by α in the nonlinear regime) increases, the mean helical phase of the island chain shifts from 0 to $\pi/2$, the mean island width decreases, and the mean decelerating electromagnetic torque first increases, attains a maximum, and then decreases. The main difference between the two regimes is that, in the linear case, the island chain is locked in a constant phase relation with respect to the error-field, whereas, in the nonlinear case, the phase relation is constantly changing.

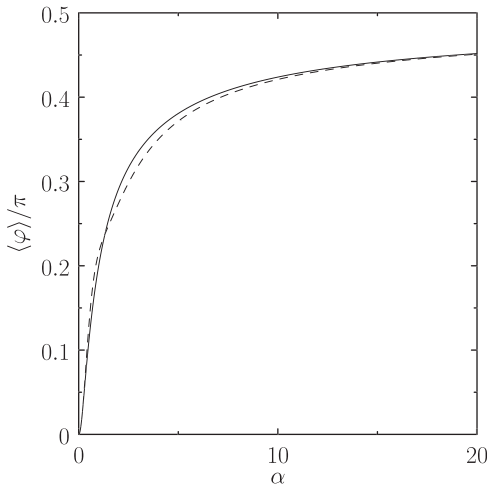

FIG. 7. Time-asymptotic nonlinear response of a rotating tokamak plasma to a resonant error-field. The solid curve shows the cycle-averaged value of φ/π calculated as a function of the plasma rotation parameter, α. The dashed curve shows the analytic approximation $\langle\varphi\rangle/\pi = \alpha^2/(1+2\,\alpha^2) - 0.1765\,\alpha^2/(1+0.4950\,\alpha^{8/3})$.

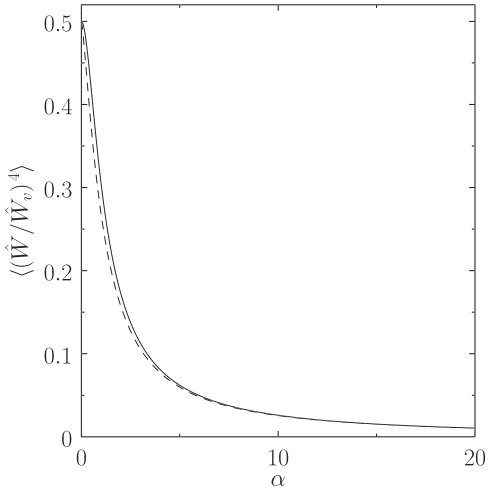

FIG. 8. Time-asymptotic nonlinear response of a rotating tokamak plasma to a resonant error-field. The solid curve shows the cycle-averaged value of $(\hat{W}/\hat{W}_v)^4$ calculated as a function of the plasma rotation parameter, α. The dashed curve shows the analytic approximation $\langle(\hat{W}/\hat{W}_v)^4\rangle = 0.5/(1+0.8624\,\alpha^{4/3})$.

Finally, because the nonlinear regime is only valid when $\hat{W} \gg 1$ (i.e., when the island width greatly exceeds the linear layer width), it follows from Eq. (81) that the time-asymptotic response of the plasma to the error-field only lies in the nonlinear regime when

$$\hat{W}_v \gg \left(\frac{1+0.8624\,\alpha^{4/3}}{0.5}\right)^{1/4}. \tag{83}$$

V. BIFURCATION THEORY

A. Response regimes

Making use of Eqs. (40)–(43), (54), and (80)–(83), we can identify four separate time-asymptotic response regimes for a rotating tokamak plasma interacting with a resonant error-field. The extents of these regimes in $\hat{\omega} - \hat{W}_v^{\,2}$ space are shown in Fig. 10.

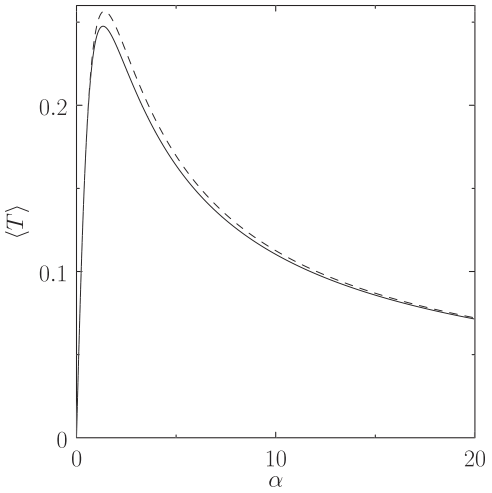

FIG. 9. Time-asymptotic nonlinear response of a rotating tokamak plasma to a resonant error-field. The solid curve shows the cycle-averaged value of T calculated as a function of the plasma rotation parameter, α. The dashed curve shows the analytic approximation $\langle T\rangle = 0.4577\,\alpha/(1+0.8546\,\alpha^{5/3})$.

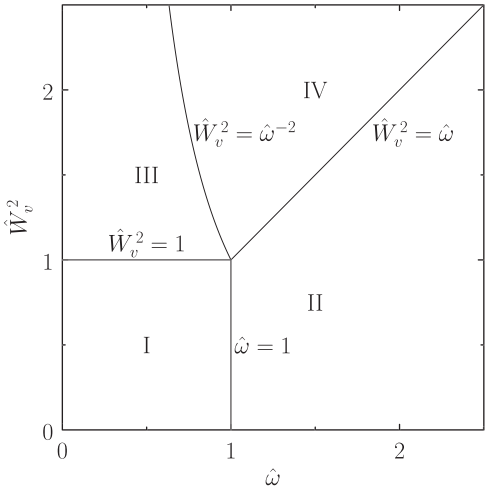

FIG. 10. Time-asymptotic response regimes for a rotating tokamak plasma interacting with a resonant error-field.

Regime I corresponds to $\hat{\omega} \ll 1$ and $\hat{W}_v^{\,2} \ll 1$. This is a linear, low-plasma-rotation response regime in which

$$\frac{\varphi}{\pi} \simeq \frac{\hat{\omega}}{\pi}, \tag{84}$$

$$\left(\frac{\hat{W}}{\hat{W}_v}\right)^4 \simeq 1, \tag{85}$$

$$T \simeq \hat{\omega}. \tag{86}$$

Regime II corresponds to $\hat{\omega} \gg 1$ and $\hat{W}_v^{\,2} \ll \hat{\omega}$. This is a linear, high-plasma-rotation response regime in which

$$\frac{\varphi}{\pi} \simeq \frac{1}{2} - \frac{\hat{\omega}^{-1}}{\pi}, \tag{87}$$

$$\left(\frac{\hat{W}}{\hat{W}_v}\right)^4 \simeq \hat{\omega}^{-2}, \tag{88}$$

$$T \simeq \hat{\omega}^{-1}. \tag{89}$$

Regime III corresponds to $1 \ll \hat{W}_v^{\,2} \ll \hat{\omega}^{-2}$. This is a nonlinear, low-plasma-rotation response regime in which

$$\frac{\langle\varphi\rangle}{\pi} \simeq 0.8235\,\alpha^2, \tag{90}$$

$$\left\langle\left(\frac{\hat{W}}{\hat{W}_v}\right)^4\right\rangle \simeq \frac{1}{2}, \tag{91}$$

$$\langle T\rangle \simeq 0.4577\,\alpha, \tag{92}$$

where $\alpha = 2\,\hat{\omega}\,\hat{W}_v/3$.

Finally, Regime IV corresponds to $\hat{W}_v^{\,2} \ll \hat{\omega}^{-2}, \hat{\omega}$. This is a nonlinear, high-plasma-rotation response regime in which

$$\frac{\langle\varphi\rangle}{\pi} \simeq \frac{1}{2} - 0.3566\,\alpha^{-2/3}, \tag{93}$$

$$\left\langle \left(\frac{\hat{W}}{\hat{W}_v} \right)^4 \right\rangle \simeq 0.5798\, \alpha^{-4/3}, \tag{94}$$

$$\langle T \rangle \simeq 0.5356\, \alpha^{-2/3}. \tag{95}$$

Expressions (40)–(42) interpolate between regimes I and II, whereas expressions (80)–(82) interpolate between regimes III and IV.

B. Toroidal torque balance

In general (or, to be more exact, in the nonlinear response regime), the time-asymptotic toroidal electromagnetic torque, $T_{\phi\,\mathrm{EM}}$, exerted by an error-field on a rotating plasma varies in time. However, the typical variation timescale is of order the rotation period, which is generally much shorter than the global viscous diffusion timescale. Hence, it is reasonable to suppose that the plasma averages over any oscillations in the torque, and responds primarily to the time-averaged torque, $\langle T_{\phi\,\mathrm{EM}} \rangle$ (see Appendix C). Note, incidentally, that the error-field also exerts a poloidal electromagnetic torque on the plasma. However, the response to this torque is largely suppressed by the strong poloidal flow damping typically present in tokamak plasmas.[6] Consequently, in the following, we shall neglect the poloidal torque.

Suppose that the change in the plasma toroidal angular velocity profile induced by the time-averaged toroidal electromagnetic torque is $\Delta\Omega_\phi(r)$. The appropriate boundary condition at the edge of the plasma is[3]

$$\Delta\Omega_\phi(a) = 0. \tag{96}$$

In other words, the plasma rotation is effectively clamped at the edge, and is not substantially modified by the error-field. Perpendicular viscosity gives rise to a localized viscous torque, acting in the vicinity of the rational surface, which opposes the error-field-induced change in the plasma rotation. This torque is written[4] (see Appendixes C and E)

$$T_{\phi\,\mathrm{VS}} = -\frac{4\pi^2 R_0^3\, \Delta\Omega_\phi(r_s)}{\int_{r_s}^{a} dr/r\, \mu(r)}. \tag{97}$$

It follows from Eq. (13) that

$$\omega = \omega_0 - n\, \Delta\Omega_\phi(r_s), \tag{98}$$

where

$$\omega_0 = m\, \Omega_{\theta 0}(r_s) - n\, \Omega_{\phi 0}(r_s). \tag{99}$$

Here, $\Omega_{\theta 0}(r)$ and $\Omega_{\phi 0}(r)$ are the poloidal and toroidal angular velocity profiles of the plasma, respectively, in the absence of the error-field. Incidentally, ω is the error-field-modified angular frequency of an island chain that is forced to co-rotate with the plasma, whereas ω_0 is the same frequency in the absence of the error-field.

In a steady state, the viscous torque acting on the plasma in the vicinity of the rational surface must balance the time-averaged electromagnetic torque, so that

$$\langle T_{\phi\,\mathrm{EM}} \rangle + T_{\phi\,\mathrm{VS}} = 0. \tag{100}$$

Equations (14), (15), (97), (98), and (100) can be combined to give the torque-balance criterion

$$\hat{\omega}_0 - \hat{\omega} = \left(\frac{\hat{W}_v}{R} \right)^4 \langle T \rangle, \tag{101}$$

where

$$\hat{\omega}_0 = \left(\frac{\delta_{\mathrm{VR}}}{r_s} \frac{\tau_R}{-\Delta'} \right) \omega_0, \tag{102}$$

$$R = \left[\frac{2^5\, (0.8227)^4}{(2.104)^6} \frac{\delta_{\mathrm{VR}}}{r_s} \left(\frac{B_\phi}{B_\theta(r_s)} \right)^2 \Big/ \int_{r_s}^{a} \frac{dr}{r} \frac{\mu(r_s)}{\mu(r)} \right]^{1/4}. \tag{103}$$

C. Bifurcation theory in linear response regime

In the two linear response regimes (i.e., regimes I and II), Eqs. (42) and (101) can be combined to give

$$\hat{\omega}_0 - \hat{\omega} = \left(\frac{\hat{W}_v}{R} \right)^4 \frac{\hat{\omega}}{1 + \hat{\omega}^2}. \tag{104}$$

The previous expression is equivalent to

$$f(x) = 0, \tag{105}$$

where

$$f(x) \equiv \gamma\, x^3 - \gamma\, x^2 + \frac{\beta}{3}\, x - \frac{1}{27}, \tag{106}$$

and

$$x = \frac{\hat{\omega}}{\hat{\omega}_0}, \tag{107}$$

$$\beta = \frac{1}{9} \left[1 + \left(\frac{\hat{W}_v}{R} \right)^4 \right], \tag{108}$$

$$\gamma = \frac{\hat{\omega}_0^2}{27}. \tag{109}$$

Here, x parameterizes the actual (i.e., in the presence of the error-field) plasma rotation, β parameterizes the amplitude of the error-field, and γ parameterizes the intrinsic (i.e., in the absence of the error-field) plasma rotation.

The numerical solution of the time-asymptotic torque-balance equation, (105), is shown in Fig. 11. It can be seen that, at fixed intrinsic plasma rotation (i.e., fixed γ), x decreases monotonically with increasing β when $\gamma < 1$. On the other hand, there is a range of x-values in which x increases with increasing β when $\gamma > 1$. It is demonstrated in Appendix B that solutions of the torque-balance equation for which the plasma rotation decreases with increasing error-field amplitude (i.e., x deceases with increasing β) are dynamically stable, whereas solutions for which the plasma rotation increases with increasing error-field amplitude (i.e.,

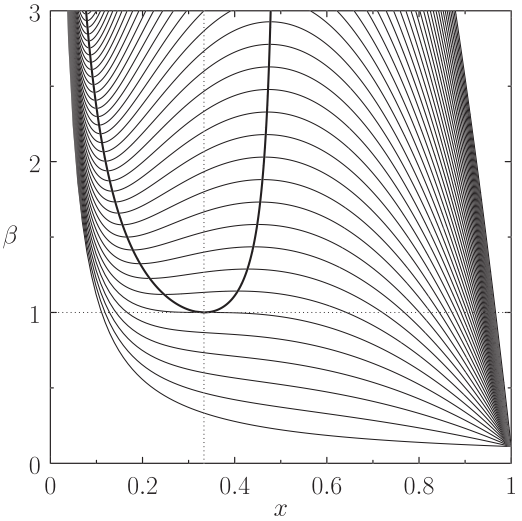

FIG. 11. Solutions of the time-asymptotic torque-balance equation in the linear response regime. The thin curves show constant-γ solutions plotted in x-β space. The curve that passes through the point $x=1/3$, $\beta=1$ corresponds to $\gamma=1$. Curves that pass below (in β) this point correspond to $\gamma<1$, and vice versa. The solutions lying inside the thick curve are dynamically unstable.

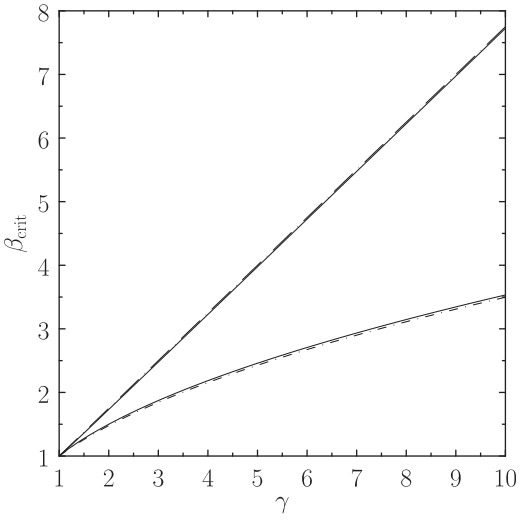

FIG. 12. Bifurcation thresholds for the solutions of the time-asymptotic torque-balance equation in the linear response regime. The upper solid curve shows the critical β value above which high-rotation solutions bifurcate to low-rotation solutions, plotted as a function of γ. Similarly, the lower solid curve shows the critical β value below which low-rotation solutions bifurcate to high-rotation solutions. The long-dashed-dotted curve shows the analytic approximation $\beta=1+3\ (\gamma\ -\ 1)/4$. The short-dashed-dotted curve shows the analytic approximation $\beta=1+(4/3)^{1/2}\ (\gamma^{1/2}-1)$.

x increases with decreasing β) are dynamically unstable.[3,4] We conclude that the general solution of the torque-balance equation exhibits a "forbidden band" of plasma rotation frequencies when $\gamma>1$ (i.e., when the intrinsic plasma rotation is sufficiently high). This band separates a branch of dynamically stable low-rotation solutions from a branch of dynamically stable high-rotation solutions. Thus, when a low-rotation solution crosses the lower boundary of the forbidden band, it becomes dynamically unstable, and there is a bifurcation to a high-rotation solution (characterized by the same values of β and γ). Likewise, when a high-rotation solution crosses the upper boundary of the forbidden band, it becomes dynamically unstable, and there is a bifurcation to a low-rotation solution.

The numerically determined critical values of β at which the aforementioned bifurcations take place are shown in Fig. 12. It can be seen that, to a good approximation, the bifurcation from the high-rotation to the low-rotation solution branch occurs when β exceeds the critical value

$$\beta_+ \simeq 1+\frac{3}{4}\,(\gamma-1). \tag{110}$$

On the other hand, the bifurcation from the low-rotation to the high-rotation solution branch occurs when β falls below the critical value

$$\beta_- \simeq 1+\left(\frac{4}{3}\right)^{1/2}\left(\gamma^{1/2}-1\right). \tag{111}$$

The previous two expressions are only valid when $\gamma>1$. For $\gamma\leq 1$, there is no forbidden band of plasma rotation frequencies, and, consequently, no bifurcations.

According to the definitions (108) and (109), the bifurcation from the high-rotation to the low-rotation solution branch occurs when the normalized vacuum island width exceeds the critical value

$$\hat{W}_{v+} \simeq \left(8+\frac{\hat{\omega}_0^2-27}{4}\right)^{1/4} R. \tag{112}$$

On the other hand, the bifurcation from the low-rotation to the high-rotation solution branch occurs when the normalized vacuum island width falls below the critical value

$$\hat{W}_{v-} \simeq \left[8+2\,(\hat{\omega}_0-\sqrt{27})\right]^{1/4} R. \tag{113}$$

In general, $\hat{W}_{v+}>\hat{W}_{v-}$. Consequently, the system exhibits hysteresis. To be more exact, once $\hat{W}_v$ has exceeded the critical value required to trigger a transition from a high-rotation solution to a low-rotation solution, its value must be significantly reduced before the reverse transition is triggered. Likewise, once $\hat{W}_v$ has fallen below the critical value required to trigger a transition from a low-rotation solution to a high-rotation solution, its value must be significantly increased before the reverse transition is triggered. The previous two expressions are only valid when $\hat{\omega}_0>\sqrt{27}$. For $\hat{\omega}_0\leq\sqrt{27}$, there are no bifurcations, and the plasma rotation varies continuously, and reversibly, with varying vacuum island width.

D. Bifurcation theory in nonlinear response regime

In the two nonlinear response regimes (i.e., regimes III and IV), Eqs. (82) and (101) can be combined to give

$$\hat{\omega}_0-\hat{\omega}=\left(\frac{\hat{W}_v}{R}\right)^4\frac{0.4577\,\alpha}{1+0.8546\,\alpha^{5/3}}, \tag{114}$$

where $\alpha=2\,\hat{\omega}\,\hat{W}_v/3$. The previous expression is equivalent to

$$g(x)=0, \tag{115}$$

where

$$g(x) \equiv \gamma' x^{8/3} - \gamma' x^{5/3} + \frac{\beta'}{2\,2^{1/3}}\, x - \frac{1}{32\,2^{1/3}}, \tag{116}$$

and

$$\beta' = \frac{1}{16}\left(1 + 0.3051\,\frac{\hat{W}_v^{\,5}}{R^4}\right), \tag{117}$$

$$\gamma' = \frac{0.3451}{32}\,\hat{W}_v^{\,5/3}\,\hat{\omega}_0^{5/3}. \tag{118}$$

Here, x parameterizes the actual (i.e., in the presence of the error-field) plasma rotation, β' parameterizes the amplitude of the error-field, and γ' parameterizes the intrinsic (i.e., in the absence of the error-field) plasma rotation.

The numerical solution of the time-asymptotic torque-balance equation, (115), is shown in Fig. 13. As before, the solution exhibits a forbidden band of plasma rotation frequencies when $\gamma' > 1$ (i.e., when the intrinsic plasma rotation is sufficiently high). This band separates a branch of dynamically stable low-rotation solutions from a branch of dynamically stable high-rotation solutions. When a low-rotation solution crosses the lower boundary of the forbidden band, a bifurcation to a high-rotation solution is triggered. Likewise, when a high-rotation solution crosses the upper boundary of the forbidden band, a bifurcation to a low-rotation solution is triggered.

The numerically determined critical values of β' at which the aforementioned bifurcations take place are shown in Fig. 14. It can be seen that, to a good approximation, the bifurcation from the high-rotation to the low-rotation solution branch occurs when β' exceeds the critical value

$$\beta'_+ \simeq 1 + \frac{12}{5^{5/3}}\,(\gamma' - 1). \tag{119}$$

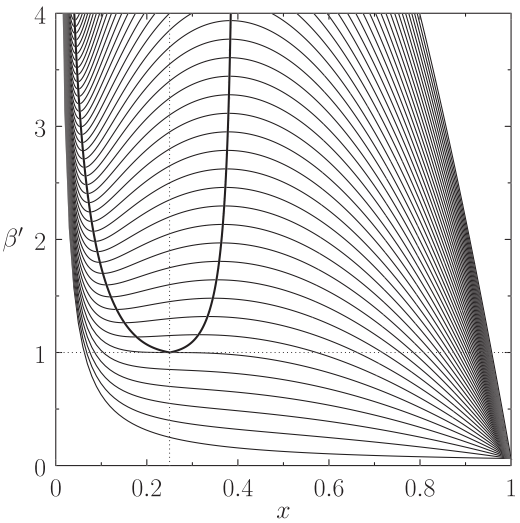

FIG. 13. Solutions of the time-asymptotic torque-balance equation in the nonlinear response regime. The thin curves show constant-γ' solutions plotted in x-β' space. The curve that passes through the point $x = 1/4$, $\beta' = 1$ corresponds to $\gamma' = 1$. Curves that pass below (in β') this point correspond to $\gamma' < 1$, and vice versa. The solutions lying inside the thick curve are dynamically unstable.

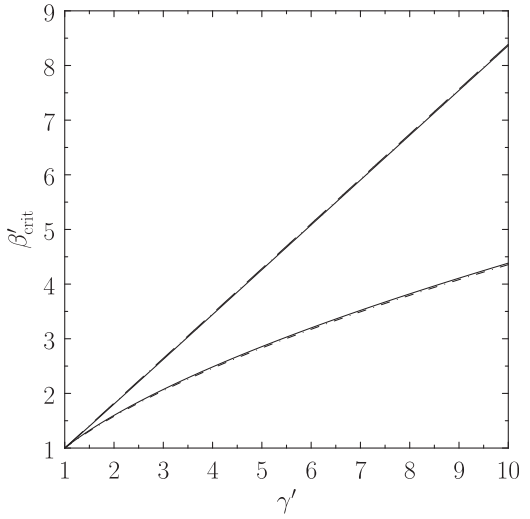

FIG. 14. Bifurcation thresholds for the solutions of the time-asymptotic torque-balance equation in the nonlinear response regime. The upper solid curve shows the critical β' value above which high-rotation solutions bifurcate to low-rotation solutions, plotted as a function of γ'. Similarly, the lower solid curve shows the critical β' value below which low-rotation solutions bifurcate to high-rotation solutions. The long-dashed-dotted curve shows the analytic approximation $\beta' = 1 + 12\,(\gamma' - 1)/5^{5/3}$. The short-dashed-dotted curve shows the analytic approximation $\beta' = 1 + (5/2)\,(\gamma'^{3/5} - 1)/(54)^{1/5}$.

On the other hand, the bifurcation from the low-rotation to the high-rotation solution branch occurs when β' falls below the critical value

$$\beta'_- \simeq 1 + \frac{5}{2\,(54)^{1/5}}\left(\gamma'^{3/5} - 1\right). \tag{120}$$

The previous two expressions are only valid when $\gamma' > 1$. For $\gamma' \leq 1$, there is no forbidden band of plasma rotation frequencies, and, consequently, no bifurcations.

According to the definitions (117) and (118), the bifurcation from the high-rotation to the low-rotation solution branch occurs when the normalized vacuum island width exceeds the critical value $\hat{W}_{v+}$, which is the positive root of

$$\hat{W}_{v+}^{\,5} - 0.4642\,\hat{\omega}_0^{5/3}\,R^4\,\hat{W}_{v+}^{\,5/3} - 6.121\,R^4 \simeq 0. \tag{121}$$

On the other hand, the bifurcation from the low-rotation to the high-rotation solution branch occurs when the normalized vacuum island width falls below the critical value $\hat{W}_{v-}$, which is the (largest) positive root of

$$\hat{W}_{v-}^{\,5} - 3.898\,\hat{\omega}_0\,R^4\,\hat{W}_{v-} + 9.875\,R^4 \simeq 0. \tag{122}$$

In general, $\hat{W}_{v+} > \hat{W}_{v-}$. Consequently, the system exhibits hysteresis. The previous two expressions are only valid when $\hat{\omega}_0 > 15.15/\hat{W}_v$. For $\hat{\omega}_0 < 15.15/\hat{W}_v$, there are no bifurcations, and the plasma rotation varies continuously, and reversibly, with varying vacuum island width.

E. Bifurcation regimes

Making use of the analysis presented in the previous two subsections, we can identify four separate bifurcation

regimes for a rotating tokamak plasma interacting with a resonant error-field. The extents of these regimes in $\hat{\omega}_0$–R space are shown in Fig. 15.

Regime I corresponds to $\hat{\omega}_0 \gg 1$ and $R \ll \hat{\omega}_0^{-1/4}$. In this regime, both the high- to low-rotation and the low- to high-rotation bifurcations take place in the linear response regime. The critical normalized vacuum island width above which the high- to low-rotation bifurcation is triggered is

$$\hat{W}_{v+} = 0.7071\, \hat{\omega}_0^{1/2} R. \tag{123}$$

This expression is obtained from Eq. (112) by taking the limit $\hat{\omega}_0 \gg 1$, and is equivalent to expression (42) of Ref. 4. Immediately before the bifurcation,

$$\hat{\omega} = \frac{1}{2}\, \omega_0, \tag{124}$$

$$\hat{W} = R. \tag{125}$$

On the other hand, the critical normalized vacuum island width below which the low- to high-rotation bifurcation is triggered is

$$\hat{W}_{v-} = 1.189\, \hat{\omega}_0^{1/4} R. \tag{126}$$

This expression is obtained from Eq. (113) by taking the limit $\hat{\omega}_0 \gg 1$. Immediately before the bifurcation,

$$\hat{\omega} = 1, \tag{127}$$

$$\hat{W} = \hat{\omega}_0^{1/4} R. \tag{128}$$

Regime II corresponds to $R \gg 1$, $\hat{\omega}_0^{-5/4}$. In this regime, both the high- to low-rotation and the low- to high-rotation bifurcations take place in the nonlinear response regime. The critical normalized vacuum island width above which the high- to low-rotation bifurcation is triggered is

$$\hat{W}_{v+} = 0.7943\, \hat{\omega}_0^{1/2} R^{6/5}. \tag{129}$$

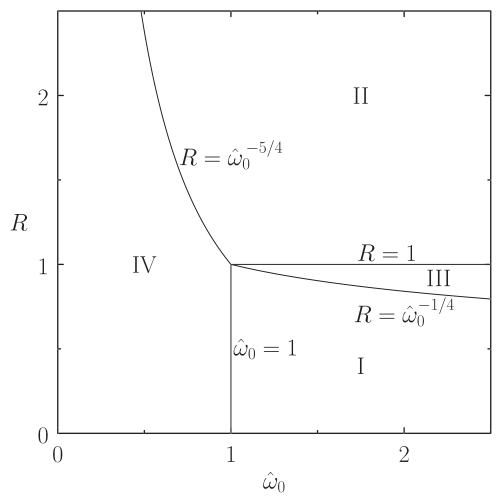

FIG. 15. Bifurcation regimes for a rotating tokamak plasma interacting with a resonant error-field.

This expression is obtained by neglecting the final term on the left-hand side of Eq. (121), and is equivalent to expression (59) of Ref. 4. Immediately before the bifurcation,

$$\hat{\omega} = \frac{2}{5}\, \hat{\omega}_0, \tag{130}$$

$$\hat{W} = 0.8567\, R^{4/5}. \tag{131}$$

On the other hand, the critical normalized vacuum island width below which the low- to high-rotation bifurcation is triggered is

$$\hat{W}_{v-} = 1.405\, \hat{\omega}_0^{1/4} R. \tag{132}$$

This expression is obtained by neglecting the final term on the left-hand side of Eq. (122). Immediately before the bifurcation,

$$\hat{\omega} = \frac{1.496}{\hat{\omega}_0^{1/4} R}, \tag{133}$$

$$\langle \hat{W} \rangle = 0.9540\, \hat{\omega}_0^{1/4} R. \tag{134}$$

Regime III corresponds to $\hat{\omega}_0^{-1/4} \ll R \ll 1$. In this regime, the high- to low-rotation bifurcation takes place in the linear response regime, whereas the low- to high-rotation bifurcation takes place in the nonlinear response regime. Thus, the critical normalized vacuum island width above which the high- to low-rotation bifurcation is triggered is

$$\hat{W}_{v+} = 0.7071\, \hat{\omega}_0^{1/2} R. \tag{135}$$

Immediately before this bifurcation,

$$\hat{\omega} = \frac{1}{2}\, \hat{\omega}_0, \tag{136}$$

$$\hat{W} = R. \tag{137}$$

On the other hand, the critical normalized vacuum island width below which the low- to high-rotation bifurcation is triggered is

$$\hat{W}_{v-} = 1.405\, \hat{\omega}_0^{1/4} R. \tag{138}$$

Immediately before this bifurcation,

$$\hat{\omega} = \frac{1.496}{\hat{\omega}_0^{1/4} R}, \tag{139}$$

$$\langle \hat{W} \rangle = 0.9540\, \hat{\omega}_0^{1/4} R. \tag{140}$$

Finally, regime IV corresponds to that part of the $\hat{\omega}_0$–R plane that is not occupied by regimes I, II, and III. There are no bifurcations in this regime.

Note that expressions (123)–(140) are only valid when the operating point in $\hat{\omega}_0$–R space lies well away from the boundaries between the various bifurcation regimes. In particular, when the boundary with regime IV is approached, expressions (123), (126), (129), and (132) must be replaced by the more general expressions (112), (113), (121), and

(122), respectively. The derivation of these general expressions represents a major extension of the analysis of Ref. 4, which only considers high- to low-rotation bifurcations, and can only deal with situations in which the operating point lies well away from the boundaries between the various bifurcation regimes.

In the regimes that exhibit bifurcations between low- and high-rotation solution branches (i.e., regimes I, II, and III), the low-rotation solutions are all characterized by $\hat{W} \sim \hat{W}_v$, whereas the high-rotation solutions are all characterized by $\hat{W} \ll \hat{W}_v$. In other words, on the low-rotation solution branch, the plasma rotation is too weak to significantly reduce the width of the island chain driven by the error-field at the rational surface. On the other hand, on the high-rotation solution branch, the plasma rotation is strong enough to significantly reduce the width of the driven island chain. Consequently, a high- to low-rotation bifurcation is invariably accompanied by a marked increase in the width of the driven island chain, whereas a low to high-rotation bifurcation is accompanied by a marked decrease.

In Fig. 15, the boundary between regimes I and IV is specified as $\hat{\omega}_0 \sim 1$. In fact, this boundary corresponds to $\beta = \gamma = 1$ (see Sec. V C). Hence, a more precise specification of the boundary is $\hat{\omega}_0 = 5.196$. Likewise, in Fig. 15, the boundary between regimes II and IV is specified as $R \sim \hat{\omega}_0^{-5/4}$. In fact, this boundary corresponds to $\beta' = \gamma' = 1$ (see Sec. V D). Hence, a more precise specification of the boundary is $R = 11.29\,\hat{\omega}_0^{-5/4}$.

VI. SUMMARY AND DISCUSSION

We have performed an in-depth investigation of the response of a rotating, quasi-cylindrical, tokamak plasma to a resonant error-field, within the context of constant-ψ, resistive-MHD theory, considerably generalizing the analysis presented previously in Refs. 3 and 4.

We find that the response of the plasma in the immediate vicinity of the rational surface to the applied error-field can be usefully visualized as a trajectory in a kind of phase-space. If the response is linear (i.e., if the driven island width is much less than the linear layer width) then the phase-space trajectory decays to a fixed point (see Sec. III B and Fig. 1). On the other hand, if the response is nonlinear (i.e., if the driven island width is much larger than the linear layer width) then the trajectory asymptotes to a limit cycle (see Sec. IV B and Fig. 3). The fixed point corresponds to a time-asymptotic linear response characterized by a non-rotating island chain of fixed width, through which the plasma at the rational surface flows (see Sec. III C). The limit cycle corresponds to a time-asymptotic nonlinear response characterized by a rotating island chain that is convected by the plasma at the rational surface, and whose width periodically falls to zero (see Sec. IV C). Each time this occurs, the helical phase of the chain (measured with respect to the error-field) decreases discontinuously by π radians. Consequently, although the phase is constantly increasing in time, it is nevertheless restricted to lie in a limited range of values.

We have derived general expressions for the mean helical phase and width of, as well as the time-averaged electromagnetic locking torque acting on, the island chain driven at the rational surface by the error-field in both the linear [see Eqs. (40)–(42)] and nonlinear [see Eqs. (80)–(82)] response regimes, and have mapped out the extents of these regimes in parameter space (see Fig. 10). We have also obtained torque-balance equations in both regimes [see Eqs. (104) and (114)]. These equations are used to determine the steady-state plasma rotation at the rational surface in the presence of the error-field. It is demonstrated that, provided the intrinsic plasma rotation is sufficiently large, the torque-balance equations possess dynamically stable low-rotation and high-rotation solution branches, separated by a forbidden band of dynamically unstable solutions (see Secs. V C and V D). It is also shown that bifurcations between the two stable solution branches are triggered as the amplitude of the error-field is varied. A low- to high-rotation bifurcation is invariably associated with a significant reduction in the width of the magnetic island chain driven at the rational surface, and vice versa. Moreover, the bifurcations exhibit considerable hysteresis. General expressions for the bifurcation thresholds have been obtained, and their respective domains of validity mapped out in parameter space (see Fig. 15).

In Appendix D, we apply the scaling analysis described in Sec. IV of Ref. 10 to the theory outlined in this paper. This analysis is appropriate to an ohmically heated tokamak plasma with (dimensionally consistent) neo-Alcator scaling of the energy confinement time. It is assumed that the momentum confinement time scales in a similar manner to the energy confinement time. The purpose of the analysis is to determine the dependance of critical parameters in the theory on the line-averaged electron number density, n_e, the mean toroidal magnetic field-strength, B_T, and the plasma major radius, R_0. We find that none of the parameters exhibit any scaling with n_e. Instead, they all scale as some power of $\zeta = B_T^{1/5} R_0^{1/4}$. [Actually, the latter result follows immediately from dimensionless scaling arguments, once it has been established that there is no density scaling.[11]] In fact,

$$\hat{W}_v \sim \left(\frac{b_r}{B_T}\right)^{1/2} \zeta^{8/3}, \tag{141}$$

$$\hat{\omega}_0 \sim \zeta^{7/3}, \tag{142}$$

$$R \sim \zeta^{-2/3}, \tag{143}$$

where b_r is the vacuum radial error-field strength at the rational surface. These scalings, in combination with Fig. 15, allow us conclude that large, high-field devices are more likely to lie in the linear bifurcation regime I, whereas small, low-field devices are more likely to lie in the nonlinear bifurcation regime II. The lack of density scaling exhibited by the previous three critical parameters means that, according to the theory outlined in this paper, none of the threshold error-field strengths at which low- to high-rotation bifurcations, or high to low-rotation bifurcations, are triggered have any dependence on n_e. Unfortunately. this prediction is in conflict with experimental observations, which indicate an approximately linear scaling of the critical field-strength needed to

trigger a high- to low-rotation bifurcation.[12–15] (More recent observations suggest a weaker density scaling in small devices.[16]) Clearly, something is missing from our theory. One possibility is error-field-induced neoclassical toroidal flow damping—see Appendix E.[10,17,18] However, it is demonstrated in Appendix D that the addition of this effect alone does not solve any problems. The only other possibility is drift effects (e.g., semi-collisional effects in the linear regime, and the ion polarization current in the nonlinear regime). In a future publication, we intend to extend the analysis presented in this paper to take drift effects into account, using the analysis of Ref. 19 as a template in the linear regime, and the analysis of Ref. 10 in the nonlinear regime.

ACKNOWLEDGMENTS

This research was funded by the U.S. Department of Energy under Contract No. DE-FG02-04ER-54742.

APPENDIX A: LINEAR RESPONSE REGIME

All quantities appearing in this appendix are defined in Sec. II. Standard asymptotic matching between the marginally stable, ideal MHD solution in the outer region (i.e., everywhere apart from the immediate vicinity of the rational surface) and the linear layer solution in the vicinity of the rational surface yields [see Eq. (6) of Ref. 4]

$$\Delta\,\Psi_s = \Delta'\,\Psi_s + 2\,m\,\Psi_v. \tag{A1}$$

For the case of the visco-resistive layer response regime [see Eqs. (9), (21), (23), (26), (27a), (27b), and (28a) of Ref. 4],

$$\Delta = \frac{\delta_{\rm VR}}{r_s}\,\tau_R\left(\frac{d}{dt} + {\rm i}\,\omega\right), \tag{A2}$$

where d/dt is the growth-rate in the plasma frame. In normalized form (given that $\Psi_s = |\Psi_s|\,{\rm e}^{-{\rm i}\,\varphi_s}$ and $\Psi_v = |\Psi_v|\,{\rm e}^{-{\rm i}\,\varphi_v}$), the previous two equations give

$$\left(\frac{d}{d\hat{t}} + {\rm i}\,\hat{\omega}\right)\left(\hat{W}^{\,2}\,{\rm e}^{-{\rm i}\,\varphi_s}\right) = -\hat{W}^{\,2}\,{\rm e}^{-{\rm i}\,\varphi_s} + \hat{W}_v^{\,2}\,{\rm e}^{-{\rm i}\,\varphi_v} \tag{A3}$$

or

$$2\,\hat{W}\,\frac{d\hat{W}}{d\hat{t}} - {\rm i}\,\hat{W}^{\,2}\,\frac{d\varphi}{d\hat{t}} + {\rm i}\,\hat{\omega}\,\hat{W}^{\,2} = -\hat{W}^{\,2} + \hat{W}_v^{\,2}\,{\rm e}^{\,{\rm i}\,\varphi}, \tag{A4}$$

where $\varphi = \varphi_s - \varphi_v$, and we have assumed that φ_v does not vary in time. Taking the real and imaginary parts of the previous equation, we obtain

$$\frac{d\hat{W}}{d\hat{t}} = \frac{\hat{W}}{2}\left(-1 + \frac{\hat{W}_v^{\,2}}{\hat{W}^{\,2}}\,\cos\varphi\right), \tag{A5}$$

$$\frac{d\varphi}{d\hat{t}} - \hat{\omega} = -\frac{\hat{W}_v^{\,2}}{\hat{W}^{\,2}}\,\sin\varphi, \tag{A6}$$

respectively.

APPENDIX B: DYNAMICAL STABILITY OF SOLUTIONS OF THE TORQUE-BALANCE EQUATION

When plasma inertia is taken into account, the torque-balance equation, (101), generalizes to give[3]

$$\frac{d\hat{\omega}}{d\hat{t}} = k\,F(\hat{\omega}), \tag{B1}$$

where

$$F(\hat{\omega}) = \hat{\omega}_0 - \hat{\omega} - \zeta\,\langle T\rangle(\hat{\omega}). \tag{B2}$$

Here, $k>0$, $\zeta = (\hat{W}_v/R)^4 > 0$, and $\langle T\rangle(\hat{\omega}) > 0$ is the normalized, time-averaged, electromagnetic torque. A stable equilibrium solution of (B1) is such that

$$F(\hat{\omega}_1) = 0, \tag{B3}$$

$$F'(\hat{\omega}_1) < 0, \tag{B4}$$

where $F'(\hat{\omega}) \equiv dF/d\hat{\omega}$. It follows that $\hat{\omega} = \hat{\omega}_1$ is a dynamically stable, steady-state solution of the generalized torque-balance equation, (B1), provided that:

$$1 + \zeta\,\langle T\rangle'(\hat{\omega}_1) > 0. \tag{B5}$$

Here, $\langle T\rangle'(\hat{\omega}) \equiv d\langle T\rangle/d\hat{\omega}$. Suppose that $\zeta \to \zeta + d\zeta$, and that the corresponding steady-state solution of (B1) changes from $\hat{\omega}_1$ to $\hat{\omega}_1 + d\hat{\omega}_1$. To first order in small quantities, we obtain

$$\frac{\delta\hat{\omega}_1}{\delta\zeta} = -\frac{\langle T\rangle(\hat{\omega}_1)}{1 + \zeta\,\langle T\rangle'(\hat{\omega}_1)}. \tag{B6}$$

It follows from (B5) that if $\hat{\omega} = \hat{\omega}_1$ is a dynamically stable, steady-state solution of the torque-balance equation then

$$\frac{\delta\hat{\omega}_1}{\delta\zeta} < 0. \tag{B7}$$

In other words, a dynamically stable solution is such that the plasma rotation (which is parameterized by $\hat{\omega}_1$) decreases with increasing error-field amplitude (which is parameterized by ζ). Conversely, if the plasma rotation increases with increasing error-field amplitude then the corresponding solution is dynamically unstable.

APPENDIX C: PLASMA TOROIDAL EQUATION OF ANGULAR MOTION

The plasma's toroidal equation of angular motion is written as[3]

$$4\pi^2\,R_0^3\left[\rho\,r\,\frac{\partial\Delta\Omega_\phi}{\partial t} - \frac{\partial}{\partial r}\left(\mu\,r\,\frac{\partial\Delta\Omega_\phi}{\partial r}\right)\right] = T_{\phi\,\rm EM}\,\delta(r - r_s). \tag{C1}$$

Here, $\Delta\Omega_\phi(r,t)$, $\rho(r)$, and $\mu(r)$ are the plasma toroidal angular velocity-shift (due to the error-field torque), mass density, and (perpendicular) viscosity profiles, respectively, whereas

$T_{\phi\,\mathrm{EM}}(t)$ is the (time-asymptotic) toroidal electromagnetic torque exerted by the error-field in the vicinity of the rational surface, $r = r_s$. The physical boundary conditions are[3]

$$\frac{\partial \Delta\Omega_\phi(0,t)}{\partial r} = \Delta\Omega_\phi(a,t) = 0, \tag{C2}$$

where a is the plasma minor radius.

Suppose that

$$T_{\phi\,\mathrm{EM}}(t) = \langle T_{\phi\,\mathrm{EM}}\rangle + \tilde{T}_{\phi\,\mathrm{EM}}\,\mathrm{e}^{\,\mathrm{i}\,\omega\,t}, \tag{C3}$$

$$\Delta\Omega_\phi(r,t) = \Delta\Omega_\phi(r) + \Delta\tilde{\Omega}_\phi(r)\,\mathrm{e}^{\,\mathrm{i}\,\omega\,t}, \tag{C4}$$

where the frequency ω is specified in Eq. (13). It follows that

$$-4\pi^2 R_0^3 \frac{d}{dr}\left(\mu\, r\, \frac{d\Delta\Omega_\phi}{dr}\right) = \langle T_{\phi\,\mathrm{EM}}\rangle\, \delta(r - r_s), \tag{C5}$$

and

$$\frac{d\Delta\Omega_\phi(0)}{dr} = \Delta\Omega_\phi(a) = 0. \tag{C6}$$

Hence,

$$\Delta\Omega_\phi(0) = \Delta\Omega_\phi(r_s)\begin{cases} 1 & r < r_s \\ \int_r^a dr/r\,\mu \big/ \int_{r_s}^a dr/r\,\mu & r > r_s, \end{cases} \tag{C7}$$

where

$$\Delta\Omega_\phi(r_s) = \frac{\langle T_{\phi\,\mathrm{EM}}\rangle}{4\pi^2 R_0^3}\int_{r_s}^a \frac{dr}{r\,\mu(r)}. \tag{C8}$$

We also have

$$-4\,\pi^2 R_0^3\left[\mathrm{i}\,\omega\,\rho\, r\,\Delta\tilde{\Omega}_\phi - \frac{d}{dr}\left(\mu\, r\,\frac{d\Delta\tilde{\Omega}_\phi}{dr}\right)\right] = \tilde{T}_{\phi\,\mathrm{EM}}\,\delta(r - r_s), \tag{C9}$$

and

$$\frac{d\Delta\tilde{\Omega}_\phi(0)}{dr} = \Delta\tilde{\Omega}_\phi(a) = 0. \tag{C10}$$

Assuming that $\omega\tau_V \gg 1$, where $\tau_V = r_s^2\,\rho(r_s)/\mu(r_s)$, we obtain

$$\Delta\tilde{\Omega}_\phi(0) \simeq \Delta\tilde{\Omega}_\phi(r_s)\begin{cases} \exp[+\mathrm{e}^{\,\mathrm{i}\,\pi/4}\sqrt{\omega\,\tau_V}\,(r - r_s)/r_s] & r < r_s \\ \exp[-\mathrm{e}^{\,\mathrm{i}\,\pi/4}\sqrt{\omega\,\tau_V}\,(r - r_s)/r_s] & r > r_s, \end{cases} \tag{C11}$$

where

$$\Delta\tilde{\Omega}_\phi(r_s) = \frac{\mathrm{e}^{-\mathrm{i}\,\pi/4}\,\tilde{T}_{\phi\,\mathrm{EM}}}{4\pi^2 R_0^3\, 2\,\mu(r_s)\,\sqrt{\omega\,\tau_V}}. \tag{C12}$$

The approach adopted in this paper, in which only the response of the plasma to the time-averaged electromagnetic torque is taken into consideration, is justified provided that

$$\left|\frac{\Delta\tilde{\Omega}_\phi(r_s)}{\Delta\Omega_\phi(r_s)}\right| \ll 1. \tag{C13}$$

According to Eqs. (C8) and (C12), this implies that

$$\frac{\tilde{T}_{\phi\,\mathrm{EM}}}{\langle T_{\phi\,\mathrm{EM}}\rangle} \ll \sqrt{\omega\,\tau_V}. \tag{C14}$$

In the linear response regime, discussed in Sec. III, $\tilde{T}_{\phi\,\mathrm{EM}} = 0$, so the above inequality is automatically satisfied. However, in the nonlinear response regime, discussed in Sec. IV, $\tilde{T}_{\phi\,\mathrm{EM}} \sim \langle T_{\phi\,\mathrm{EM}}\rangle$. In this case, the inequality can only be satisfied if

$$\omega\,\tau_V \gg 1. \tag{C15}$$

Let us estimate the typical value of $\omega\tau_V$. In the intermediate plasma rotation limit, in which $\alpha \sim 1$, where [see Eqs. (22), (24), and (56)] $\alpha \sim \omega\tau_R W_v/r_s$, we find that

$$\omega\,\tau_V \sim \frac{r_s}{W_v}\,\frac{\tau_V}{\tau_R}, \tag{C16}$$

or [see Eqs. (22) and (103)]

$$\omega\,\tau_V \sim \frac{1}{\hat{W}_v}\,\frac{r_s}{\delta_{\mathrm{VR}}}\,\frac{\tau_V}{\tau_R} \sim \frac{1}{\hat{W}_v\,R^4}\left[\frac{B_\phi}{B_\theta(r_s)}\right]^2\frac{\tau_V}{\tau_R}. \tag{C17}$$

Now, according to the analysis of Sec. V E, we have $\hat{W}_v \sim R \sim 1$ at the boundary between bifurcation regimes I, II, III, and IV (see Fig. 15), so, in this case,

$$\omega\,\tau_V \sim \left[\frac{B_\phi}{B_\theta(r_s)}\right]^2\frac{\tau_V}{\tau_R}. \tag{C18}$$

Thus, (C15) yields

$$\left[\frac{B_\phi}{B_\theta(r_s)}\right]^2\frac{\tau_V}{\tau_R} \gg 1. \tag{C19}$$

In conventional, large aspect-ratio, ohmically heated, tokamak plasmas, $1/6 \lesssim \tau_V/\tau_R \lesssim 1$, whereas $B_\phi/B_\theta(r_s) \sim 6$.[4] Hence, the previous inequality is easily satisfied, implying that the neglect of the response of the plasma to the time-varying component of the electromagnetic torque is justified.

APPENDIX D: SCALING ANALYSIS

In this appendix, we apply the scaling analysis described in Sec. IV of Ref. 10 to the theory outlined in this paper. The analysis is appropriate to an ohmically heated tokamak plasma with (dimensionally consistent) neo-Alcator scaling of the energy confinement time. It is assumed that the momentum confinement time scales in a similar manner to the energy confinement time. According to the analysis,

$$\hat{W}_v \sim \left(\frac{b_r}{B_T}\right)^{1/2}\zeta^{8/3}, \tag{D1}$$

$$\hat{\omega}_0 \sim \zeta^{7/3}, \tag{D2}$$

$$R \sim \zeta^{-2/3}, \tag{D3}$$

$$\frac{\tau_V}{\tau_D} \sim \zeta^{-2}, \tag{D4}$$

where

$$\zeta = B_T^{1/5} R_0^{1/4}. \tag{D5}$$

Here, b_r is the vacuum radial error-field at the rational surface, B_T the mean toroidal magnetic field-strength, and R_0 the plasma major radius. It is interesting to note that none of the above quantities exhibit any dependence on the line-averaged electron number density, n_e.

The critical error-field amplitude above which the high- to low-rotation bifurcation is triggered in bifurcation regimes I and III of Sec. V E [which follows from Eq. (123)] scales as[10]

$$\left(\frac{b_r}{B_T}\right)_+ \sim \zeta^{-13/3}. \tag{D6}$$

The critical error-field amplitude above which the high- to low-rotation bifurcation is triggered in bifurcation regime II [which follows from Eq. (129)] scales as

$$\left(\frac{b_r}{B_T}\right)_+ \sim \zeta^{-23/5}. \tag{D7}$$

Finally, the critical error-field amplitude below which the low- to high-rotation bifurcation is triggered in bifurcation regimes I, II, and III [which follows from Eq. (126)] scales as

$$\left(\frac{b_r}{B_T}\right)_- \sim \zeta^{-11/2}. \tag{D8}$$

It can be seems that none of the above critical error-field strengths exhibit any scaling with n_e.

According to the analysis of Appendix E, error-field-induced neoclassical toroidal flow damping must be taken into account in the bifurcation analysis whenever

$$\left(\frac{\tau_V}{\tau_D}\right)^{1/2} \hat{W}_v^{\,2} \gg 1 \tag{D9}$$

or

$$\frac{b_r}{B_T} \gg \left(\frac{b_r}{B_T}\right)_{\rm crit}, \tag{D10}$$

where

$$\left(\frac{b_r}{B_T}\right)_{\rm crit} \sim \zeta^{-13/3}. \tag{D11}$$

If the inequality (D10) is satisfied then the critical error-field strengths (D6), (D7), and (D8) become

$$\left(\frac{b_r}{B_T}\right)_+ \sim \zeta^{-13/3}, \tag{D12}$$

$$\left(\frac{b_r}{B_T}\right)_+ \sim \zeta^{-15/3}, \tag{D13}$$

$$\left(\frac{b_r}{B_T}\right)_- \sim \zeta^{-20/3}, \tag{D14}$$

respectively. Note, again, that none of the above critical values exhibit any scaling with n_e.

APPENDIX E: EFFECT OF NEOCLASSICAL TOROIDAL FLOW DAMPING

Equation (C5) can be generalized to give[10,17,18]

$$4\pi^2 R_0^3 \left[\rho\, \nu_\phi\, r\, \Delta\Omega_\phi - \frac{d}{dr}\left(\mu\, r\, \frac{d\Delta\Omega_\phi}{dr}\right)\right] = \langle T_{\phi\,\rm EM}\rangle\, \delta(r - r_s), \tag{E1}$$

and

$$\frac{d\Delta\Omega_\phi(0)}{dr} = \Delta\Omega_\phi(a) = 0, \tag{E2}$$

where $\nu_\phi(r)$ is the error-field-induced neoclassical toroidal flow damping rate. In the limit that $\tau_V\, \nu_{\phi s} \ll 1$, where $\nu_{\phi s} = \nu_\phi(r_s)$, we obtain the solution specified in Eqs. (C7) and (C8). In the opposite limit, we get

$$\Delta\Omega_\phi(r) \simeq \Delta\Omega_\phi(r_s) \begin{cases} \exp\left[+\sqrt{\nu_{\phi s}\,\tau_V}\,(r - r_s)/r_s\right] & r < r_s \\ \exp\left[-\sqrt{\nu_{\phi s}\,\tau_V}\,(r - r_s)/r_s\right] & r > r_s, \end{cases} \tag{E3}$$

where

$$\Delta\Omega_\phi(r_s) = \frac{\langle T_{\phi\,\rm EM}\rangle}{4\pi^2 R_0^3\, 2\, \mu(r_s)\, \sqrt{\nu_{\phi s}\,\tau_V}}. \tag{E4}$$

The toroidal torque-balance equation takes the form

$$\langle T_{\phi\,\rm EM}\rangle + T_{\phi\,\rm VS} = 0, \tag{E5}$$

where

$$T_{\phi\,\rm VS} = 4\pi^2 R_0^3 \left[\mu\, r\, \frac{d\Delta\Omega_\phi}{dr}\right]_{r_s-}^{r_s+}. \tag{E6}$$

Combining the $\tau_V\, \nu_{\phi s} \ll 1$ and $\tau_V\, \nu_{\phi s} \gg 1$ solutions, we obtain the following approximate expression:

$$T_{\phi\,\rm VS} \simeq -4\pi^2 R_0^3\, \mu(r_s) \left[1 \Big/ \int_{r_s}^{a} \frac{dr}{r}\, \frac{\mu(r_s)}{\mu(r)} + 2\sqrt{\nu_{\phi s}\,\tau_V}\right] \Delta\Omega_\phi(r_s). \tag{E7}$$

Assuming that the neoclassical toroidal flow damping lies in the so-called $1/\nu$ regime, we expect the flow damping rate to scale as the square of the error-field amplitude.[10,17,18] Thus, we can write

$$\nu_{\phi s} = \frac{\hat{W}_v^{\,4}}{\tau_D} \Big/ \left[2 \int_{r_s}^{a} \frac{dr}{r}\, \frac{\mu(r_s)}{\mu(r)}\right]^2, \tag{E8}$$

where the flow damping timescale τ_D is independent of the error-field amplitude. It follows that [cf. Eq. (97)]:

$$T_{\phi\,\mathrm{VS}} = -\frac{4\pi^2 R_0^3\,\Delta\Omega_\phi(r_s)}{\int_{r_s}^a dr/r\,\mu(r)}\left[1+\left(\frac{\tau_V}{\tau_D}\right)^{1/2}\hat{W}_v^{\,2}\right]. \tag{E9}$$

Thus, the torque-balance equation (101) generalizes to give

$$\hat{\omega}_0 - \hat{\omega} = \frac{\left(\hat{W}_v/R\right)^4}{\left[1+\left(\tau_V/\tau_D\right)^{1/2}\hat{W}_v^{\,2}\right]}\,\langle T\rangle. \tag{E10}$$

[1]P. H. Rutherford, Phys. Fluids **16**, 1903 (1973).
[2]Z. Chang and J. D. Callen, Nucl. Fusion **30**, 219 (1990).
[3]R. Fitzpatrick, Nucl. Fusion **33**, 1049 (1993).
[4]R. Fitzpatrick, Phys. Plasmas **5**, 3325 (1998).
[5]H. P. Furth, J. Killeen, and M. N. Rosenbluth, Phys. Fluids **6**, 459 (1963).
[6]T. H. Stix, Phys. Fluids **16**, 1260 (1973).
[7]Q. Hu, Q. Yu, R. Rao, Y. Ding, X. Hu, G. Zhuang, and J-TEXT Team, Nucl. Fusion **52**, 083011 (2012).
[8]B. Rao, Y. H. Ding, A. M. Hu, W. F. Shi, X. Q. Zhang, M. Zhang, X. S. Jin, J. Y. Nan, K. X. Yu, G. Zhuang, and J-TEXT Team, Phys. Lett. A **377**, 315 (2013).
[9]Q. Hu, B. Rao, Y. Ding, G. Zhuang, W. Jin, and X. Hu, Phys. Plasmas **20**, 092502 (2013).
[10]R. Fitzpatrick, Plasma Phys. Controlled Fusion **54**, 094002 (2012).
[11]J. W. Conner and J. B. Taylor, Nucl. Fusion **17**, 1047 (1977).
[12]R. J. Buttery, M. De' Benedetti, D. A. Gates, Yu. Gribov, T. C. Hender, R. J. La Haye, P. Leahy, J. A. Leuer, A. W. Morris, A. Santagiustina, J. T. Scoville, B. J. D. Tubbing, JET Team, COMPASS-D Research Team, and DIII-D Team, Nucl. Fusion **39**, 1827 (1999).
[13]R. J. Buttery, M. De Benedetti, T. C. Hender, and B. J. D. Tubbing, Nucl. Fusion **40**, 807 (2000).
[14]S. M. Wolfe, I. H. Hutchinson, R. D. Granetz, J. Rice, A. Hubbard, A. Lynn, P. Phillips, T. C. Hender, and D. F. Howell, Phys. Plasmas **12**, 056110 (2005).
[15]R. C. Wolf, W. Biel, M. F. M. de Bock, K. H. Finken, S. Günter, G. M. D. Hogeweij, S. Jachmich, M. W. Jakubowski, R. J. E. Jaspers, A. Krämer-Flecken, H. R. Koslowski, M. Lehnen, Y. Liang, B. Unterberg, S. K. Varshney, M. von Hellermann, Q. Yu, O. Zimmermann, S. S. Abdullaev, A. J. H. Donné, U. Samm, B. Schweer, M. Tokar, E. Westerhof, and TEXTOR Team, Nucl. Fusion **45**, 1700 (2005).
[16]N. Wang, B. Rao, Q. Hu, Y. Ding, Z. Chen, L. Gao, W. Jin, B. Yi, W. Zeng, Q. Li, Y. Liu, H. Xu, G. Zhuang, Y. Pan, and J-TEXT Team, Nucl. Fusion **54**, 064014 (2014).
[17]A. J. Cole, C. C. Hegna, and J. D. Callen, Phys. Plasmas **15**, 056102 (2008).
[18]K. Shaing, Phys. Plasmas **10**, 1443 (2003).
[19]A. Cole and R. Fitzpatrick, Phys. Plasmas **13**, 032503 (2006).